

Real Time Measurement System for Digital Glass Shaping Processes

Matthew Morgan, Balark Tiwari, Cindy Huang, Nudrat Nawal, Nishan Khadka, Edward C. Kinzel, and Robert G. Landers

Department of Aerospace and Mechanical Engineering
University of Notre Dame
Notre Dame, Indiana, 46556-4634

Abstract

In this paper we will discuss our work in developing real time sensing of the glass shaping process. A real time control system allows the data to be temporally and spatially registered to the laser power and the tool position and velocity. An infrared camera senses the temperature distribution of the work zone to ensure its formability. A visual camera records images of the glass shaping process and tracks the tool position. This information provides the true plunge depth. A three-axis force sensor is also integrated into the control system. This data will be used to determine the correlation between material displacement and forming forces. We conducted a series of experiments to model the shaping process, in which both velocity and temperature step changes are implemented to analyze the system response. An increase in the glass temperature decreases the glass viscosity, ultimately decreasing the glass force response. An increase in scan velocity generally increases the amount of material interacting with the shaping tool per unit time, thus increasing the glass force response.

Introduction

The current state of optical manufacturing is limited by the time-consuming and costly nature of subtractive techniques utilized to reach the desired accuracies necessary for intended functionality. Another approach to optical manufacturing is through the use formative shaping techniques, which are neither subtractive nor additive. These processes are used in large batch, low tolerance applications. The use of glass shaping in tight tolerance applications has limited development relative to more common techniques [1]. However, the selection of shaping as a main manufacturing method for glass artisans gives reason to pursue the development of glass shaping processes in automated applications. Glass artisans use a combination of tools to sculpt or blow the material. Similarly, a small graphite tool can be used to plow the surface of heated glass. Combining shaping control with glass additive manufacturing techniques expands the geometric capabilities of optical manufacturing.

A proven technique for glass additive manufacturing is digital glass forming, in which a glass filament is deposited onto a heated substrate via interaction with a fiber laser. The system shown in Figure 1 features three linear actuators that enable the formation of unique geometries

such as lattices, chimneys, and cylinders. This process is continually monitored by a thermal camera to ensure ideal glass flow conditions via a temperature control algorithm. Additionally, an optical point sensor may be used following track deposition to identify inaccuracies in the deposition, allowing for adjustments of subsequent track positions.

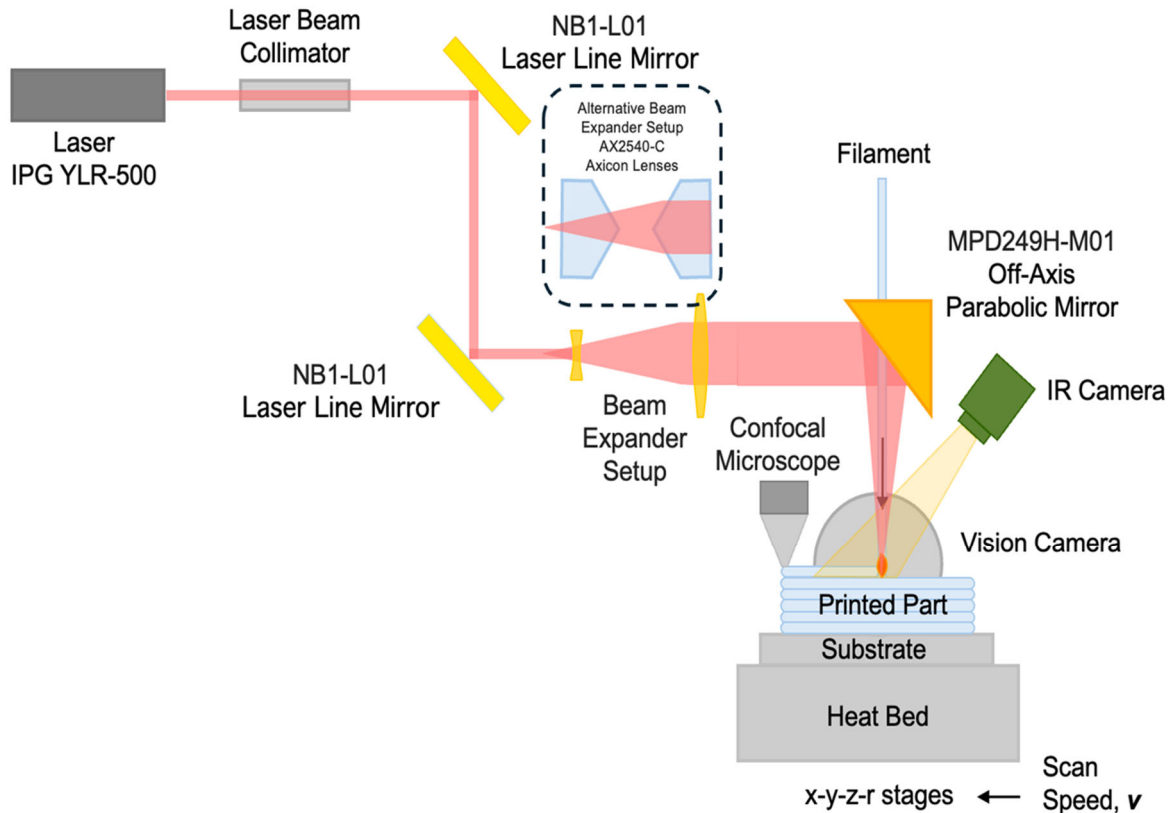


Figure 1: Laser-enabled glass deposition schematic.

The system used for digital glass forming depicting in Figure 1 is expanded in these experiments to support shaping experiments. A glass filament is no longer fed into the work zone, but rather the laser cone is used to heat the work zone to a workable temperature to interact with a graphite shaping tool. The tool is oriented along the glass substrate such that a plowing force is directly parallel to one axis, and a plunging force is directly parallel to another (see Figure 2). A force sensor utilizes strain gauges to relate the displacement of the sensor body to an applied force. As the aluminum housing is displaced, so are the strain gauges, causing an increase in the gauge resistance. These gauges output an electrical signal indicative of the strain, which can be related to the Young's Modulus of the housing to determine force. While these experiments feature linear motion, future experiments will be performed where the third axis of the force sensor will support the fabrication of increasingly complex optical components.

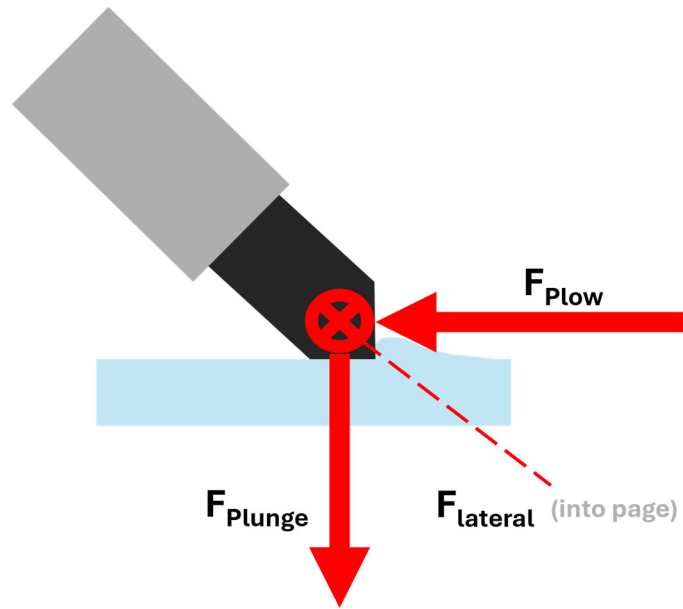


Figure 2: Coordinate system for shaping operations.

This paper demonstrates the feasibility of tight tolerance glass shaping. A similar setup to the digital glass forming process is used, in which the fiber laser brings glass to a softened state and the tool plunges into the material where the linear actuators move the glass sample such that the glass is plowed by the stationary tool tip (see Figure 3). Investigations into the workable temperature of the glass sample, plowing speed, and plowing depth were combined to identify the reactionary forces from the glass. By maintaining a constant net force in the work zone, it is theorized that glass can be shaped with high repeatability and accuracy.

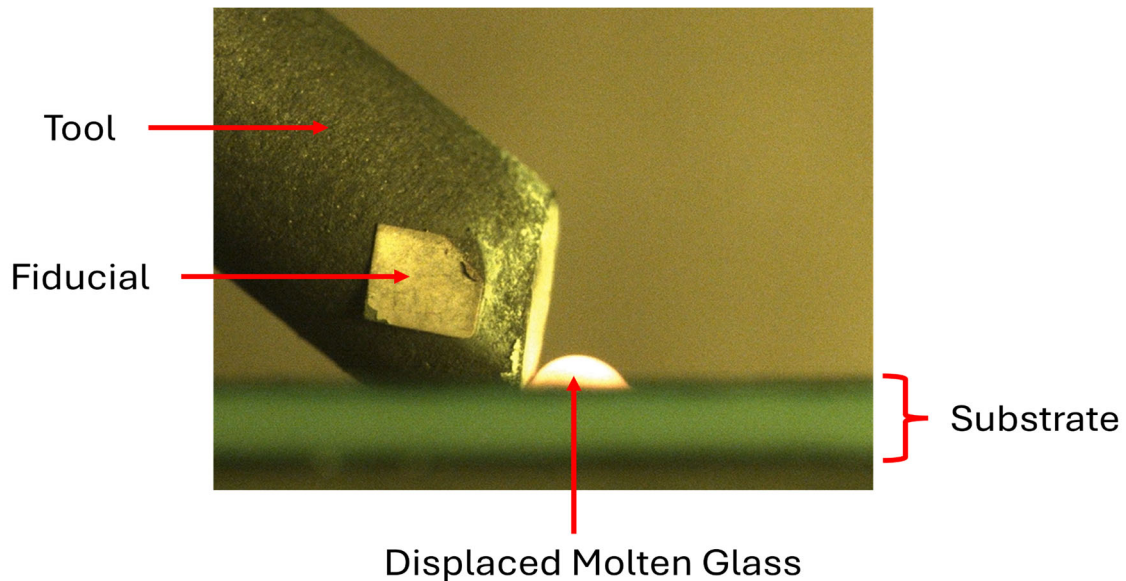


Figure 3: Displaced melt pool from plowing operation.

Shaping Force Process Model

The process parameters affecting the shaping forces are substrate velocity, plunge depth, and glass temperature. The process of shaping molten glass can be described as a first order spatial dynamic system between the shaping forces and the process parameters. In the spatial realm, a first order system is described by the gain K and spatial constant λ . A standard equation for the force response is

$$F(x) = F_i e^{-\frac{x}{\lambda}} + KA - KAe^{-\frac{x}{\lambda}} \quad (1)$$

where $F(x)$ is the current force, F_i is the initial steady value, x is the position along the substrate where $x = 0$ is the position where F_i occurs, i.e., $F(0) = F_i$, and A is the step change magnitude.

The gain is

$$K = \frac{F_f - F_i}{\Delta U} \quad (2)$$

where F_f is the final steady value and ΔU is the change in process parameter. For the experiments presented later in this paper, the process parameter will be either temperature or velocity. The spatial constant λ is a measure of the distance required for the shaping force to react after a change in the process parameter. The spatial constant is

$$\lambda = x_{63} \quad (3)$$

such that x_{63} is the position where the shaping force has reached 63% the final steady state value (see Figure 4).

In this setup, the shaping force at that time is

$$F_{63} = 0.63 \left(\frac{F_f - F_i}{F_i} \right) \quad (4)$$

where $F_{63} = F(x_{63})$. By determining these model parameters, it is possible to predict the force response of a system given the same initial conditions.

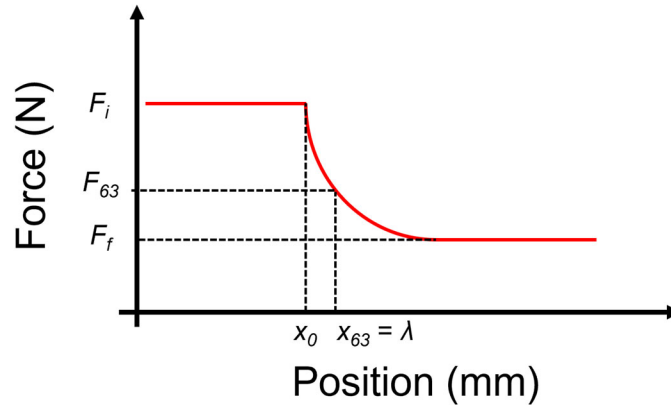


Figure 4: Force response model for an arbitrary change.

At steady state, the shaping force response will be shown to have a cyclic behavior that can be described by a spatial frequency. The tool tip repeatedly must overcome collections of displaced glass behind the tool before this material faces enough force to be pushed outward and away from the shaped track. Thus, the dynamic model above simplifies the shaping force response by predicting an average force during steady state rather than continued oscillations. More experimentation needs to be performed to accurately characterize the frequency response; however, presently the spatial frequency is estimated by

$$T_s = \frac{\sum_{i=0}^{n-1} (x_{i+1} - x_i)}{n} \quad (5)$$

where T_s is the average displacement between peaks such that spatial frequency f_s is its inverse, n is the number of peaks in a steady state region and x_i is the position of a peak. Figure 5 depicts a more accurate shaping force response for this system with an inclusion of a spatial frequency.

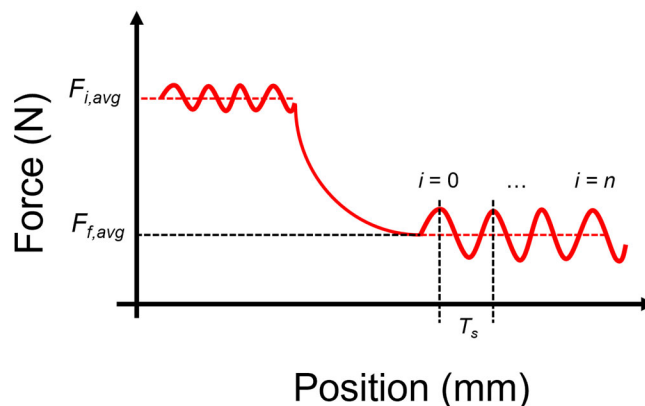


Figure 5: Force response model with frequency component.

Experimental Methods

Force Collection Setup

Connected to an upper breadboard supporting a variety of data collection equipment, an ATO 3-axis force sensor (ATO-LCMA-DYDW-0) with a 200 N capacity extends downward towards the heatbed. A series of aluminum posts are included to minimize any rotational movement of the setup such that force at the tool tip is directly transmitted to the transducer. However, there are no posts between the tool tip and sensor input, as this ensures the load is fully supported by the sensor. Ceramic posts thermally isolate the sensor from the heat of the focal point which reaches upwards of 1000°C during testing. A fusible glass (BE011630F_C) from Ed Hoy's Art & Glass Supplies with dopant impurities allow the glass to be workable with the fiber laser used in the digital glass forming setup. The laser focal point sits 20 mm above the substrate such that the laser expands to a 5 mm diameter spot size on the substrate surface compatible with the tool tip width.

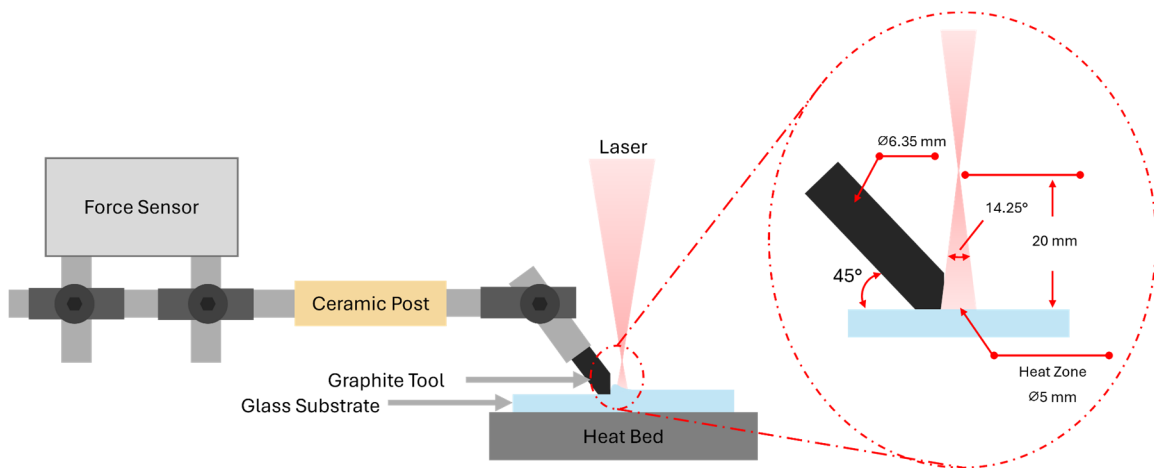


Figure 6: Schematic of shaping setup and tool positioning.

Tool Tracking Setup

A FLIR Backfly S BFS3 camera is positioned behind the force collection setup to aid in the visual identification of the fabrication process. A fiducial is attached to the tool and can be detected by the camera to relate the initial and current tool positions along the direction of tool motion.

The detection program isolates an area of pixels where the fiducial should be within the image and then applies a gray scale to highlight the white sticker. Utilizing the MATLAB Image Processing Toolbox, the program searches for a set of at least 300 connected pixels white in color. The program then fits a square to that area of pixels and performs geometric calculations to determine the fiducial's centroid position.

In another specified region, the program scans vertically for a horizontal line of pixels with a specified grey color. Once that shape is detected, a rectangle is applied to the area, to which the top end of the rectangle is the substrate surface.

At the specified time of plunging, the distance between the centroid and rectangle edge maps the current pixel distance to 0 mm. While plunging, the tool is beneath the substrate surface, where the distance is known as the plunge depth. The pixel distance is converted to millimeters with a conversion factor based on the camera distance from the focal point, and then mapped based on the assigned zero point.

To track the tool displacement along the plow axis, only the centroid of the fiducial is needed. At the time of plunging, the current pixel location is set at 0 mm for the plow axis defined in Figure 2. As the glass pushes against the tool, the tool moves backward, which is assigned a positive displacement in the plow coordinate system. This process is conducted for every frame such that the plunge depth and plow displacement are constantly tracked. An example image frame is provided in Figure 7.

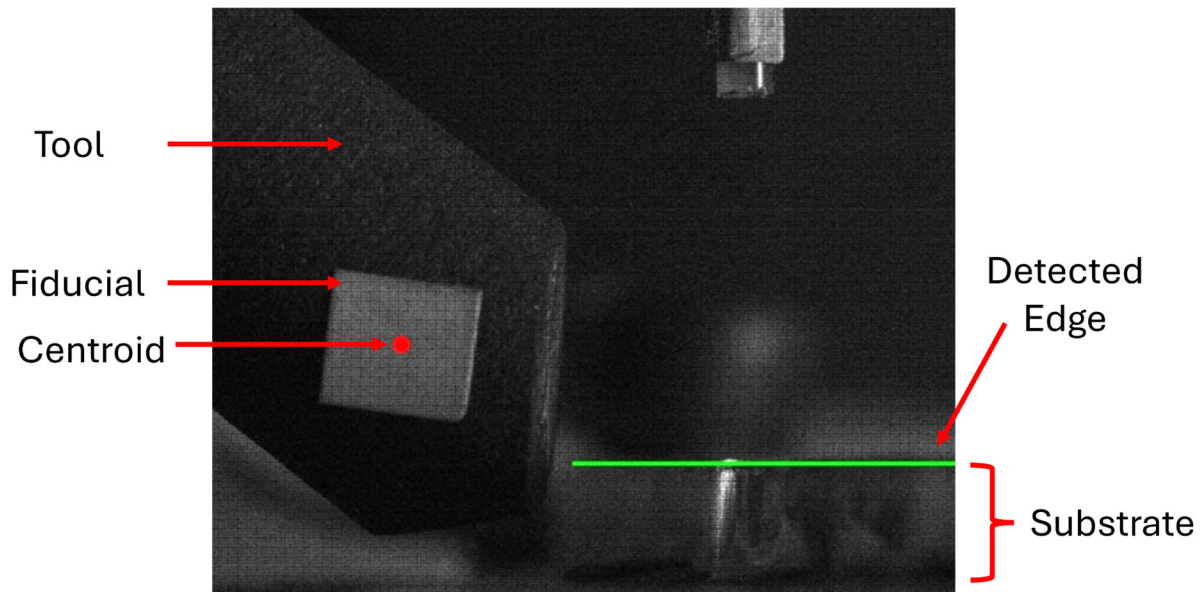


Figure 7: Example image frame of tool tracking process.

Experimental Procedure

In each experiment, the substrate is raised to 20 mm below the laser focal point. At this position, the cone-shaped laser beam expands to a 5 mm diameter on the substrate and does not intersect the tool. The shaping tool height is set such that the bottom face is 0.5 mm above the substrate surface. The laser is commanded to bring the heat zone to a desired reference

temperature, and the substrate is raised by 3 mm such that the tool plunges into the viscous glass. Once the prior motion is complete, the substrate is moved towards the shaping tool in the positive plowing direction (see Figure 2). The substrate is moved 20 mm in total, with a parameter step 10 mm into this motion. Following the 20 mm of motion, the substrate is lowered 3 mm to bring the tool back to its original position as shown in Figure 8. During this procedure, the force sensor and visual camera continuously collect data at a rate of 10 Hz. Additionally, the thermal camera, also sampled at 10 Hz, is integrated into the system to maintain acceptable temperature ranges at the work zone (see Figure 9).

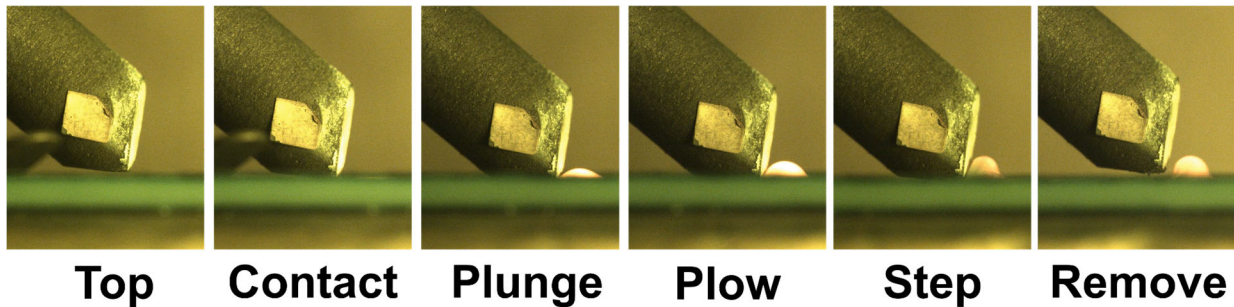


Figure 8: Standardized motion plan for shaping experiments.

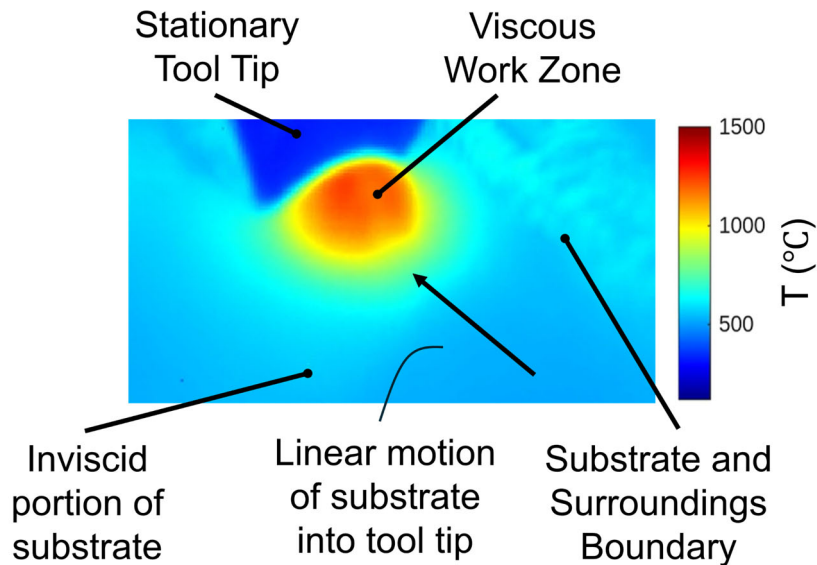


Figure 9: Thermal image of shaping operation.

Experimental Results

Response to Temperature

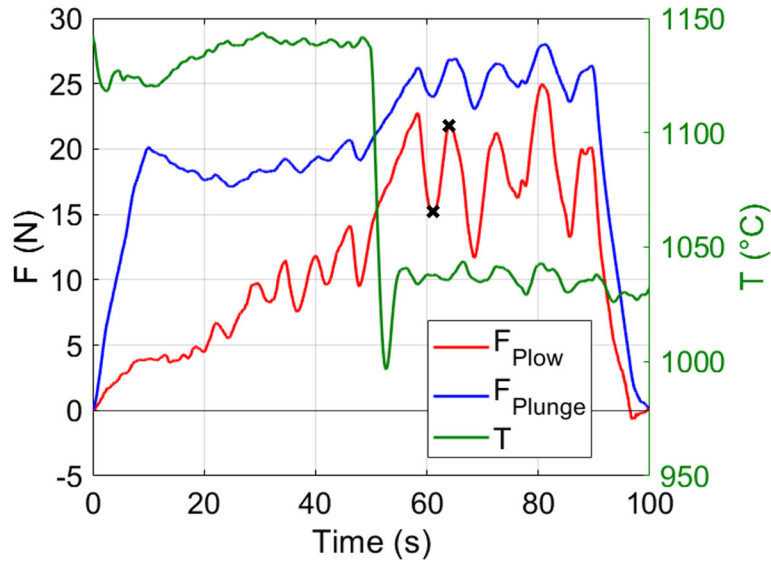


Figure 10: Plot of force (N) versus time (s) for Experiment 1. The black X's correspond to the frames in Figure 10.

The first experiment investigates the dynamic response of shaping forces to temperature. The reference temperature is initially 1100°C and is changed to 1000°C at 10 mm. The temporal responses of the shaping forces and measured temperature are shown in Figure 10. The tool plunges into the glass from roughly 0 to 10 sec at a velocity of 0.5 mm/s. During the plunge, the shaping forces increase linearly as the tool moves into a quasi-molten region of glass. The plunge force decreases slightly when shaping starts as the tool moves into a fully molten region of glass and then it becomes constant. The plough force is initially constant as the tool moves into the molten region of glass and then increases; however, it begins to oscillate.

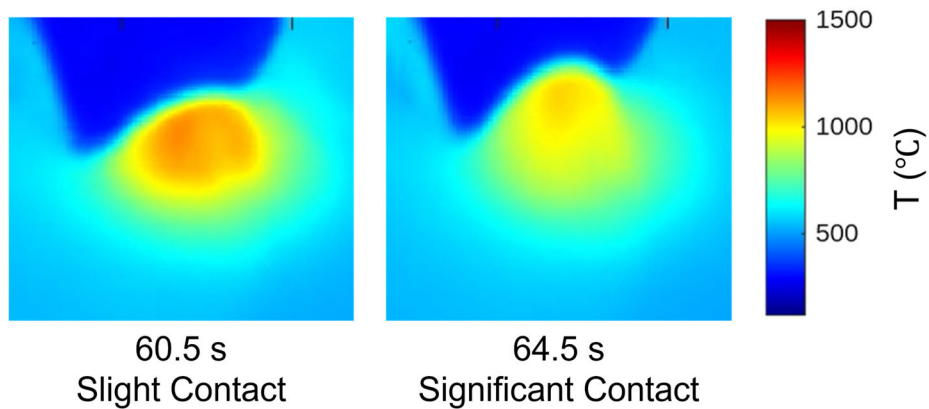


Figure 11: Thermal visualization of displaced material collection cycle.

The thermal camera (Figure 11) shows that displaced material gradually collects in front of the tooltip because the tool geometry is designed to dig into the molten glass. This increased amount of glass directly in front of the tool tip now receives less thermal energy per unit volume, as indicated by the yellow region in right image of Figure 11. This glass now resists interaction with the tool tip, thus pushing the tool tip away from the region. Then, this region receives more thermal energy per unit volume, increasing glass viscosity, to which the cycle can then repeat. The relationship between temperature and viscosity of soda lime glasses is quantified in Figure 12.

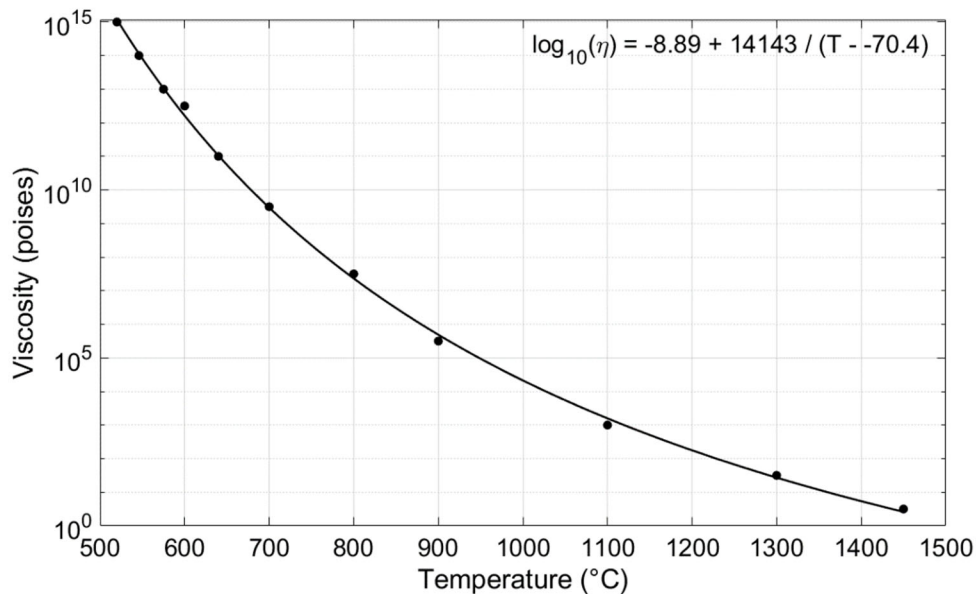


Figure 11: Viscosity as a function of temperature for soda lime glass. [2]

In Figure 13, the shaping forces, measured temperature, plunge depth, and the tool’s plow-axis displacement are shown versus displacement along the shaped feature, in this case a single trench. There is a color bar on top of the graph indicating where the temperature step occurred. The displacements are measured by processing the images of the fiducial centroid motion using the visual camera. The plunge depth increases rapidly as the tool moves into the molten region and then increases slightly during ploughing until leveling off. During the steady state regions before and after the step change in reference temperature, both force responses have an oscillatory behavior. This is due to the repeated glass viscosity changes as material collects onto the tool tip as shown in Figure 11. These oscillations are seen in the plow-axis tool displacement. The tool compliance amplifies the shaping force oscillations, which is especially obvious in the ploughing position 12 to 20 mm. In Figure 13, it is evident the positions marked with a black X correspond to areas of lower and higher tool displacements, respectively. Thus, as confirmed by the thermal imaging in Figure 11, areas where there is less material to interact with heats up to higher temperatures than areas where the tool is ploughing more material.

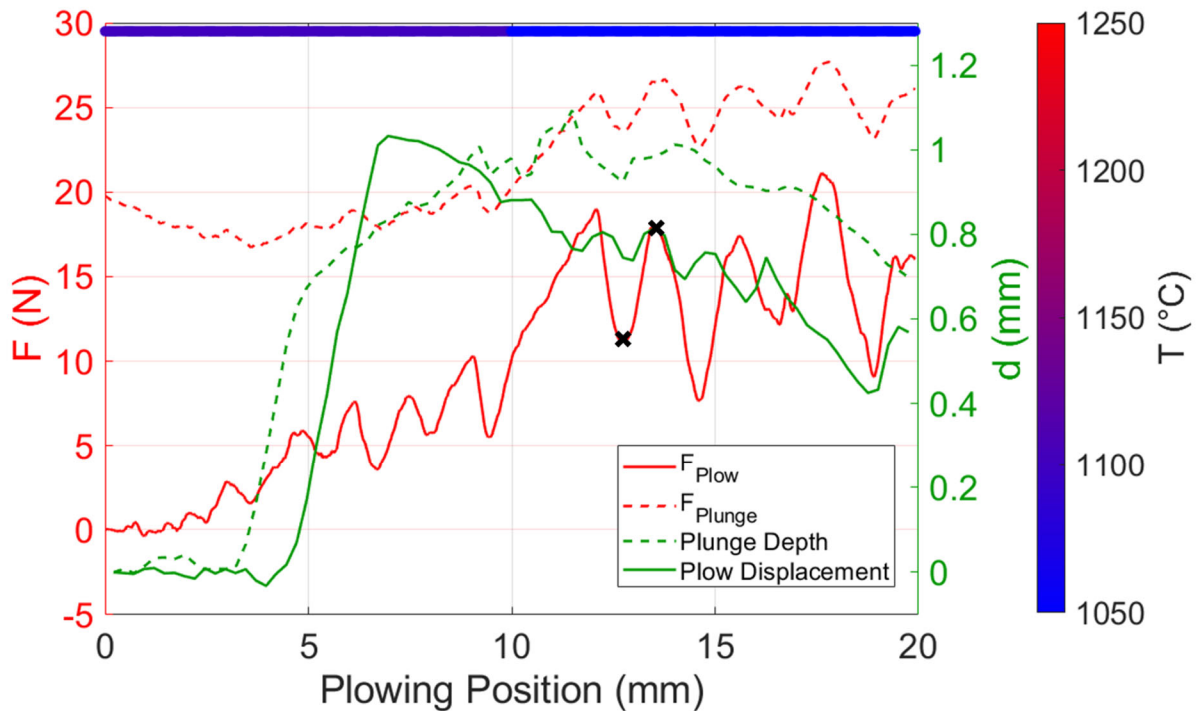


Figure 13: Plot of force (N) and displacement (mm) versus plowing position (mm) for Experiment 1. The black X's correspond to the frames in Figure 10.

Experiment 2 was similar to Experiment 1; however, the initial reference temperature was 1200°C and then decreased to 1100°C. Figure 14 shows the shaping forces, measured temperature, plunge depth, and the tool's plow-axis displacement versus displacement along the shaped feature for this experiment. The trends seen in Experiment 1 are present in this test as well. One notable behavior is the tool displacement once plowing begins. For plow-axis displacement, as the substrate moves into the tool, force is initialized on the tool, causing that displacement to increase significantly. For the plunge depth, the tool is moving from a space where only a portion of the glass interacted with the laser to a newly heated region. Thus, there is less resistance to shaping and the tool dives deeper into the substrate. When the temperature is dropped at 10 mm, the tool appears to displace less in the plow-axis direction, and plunge deeper. This is explained by the presence of the glass blob in front of the tool that geometrically limits removal despite the glass being less viscous. Another interesting observation is the near zero tool displacement in both directions for the first 4 millimeters of linear travel. The laser focal point sits slightly in front of the tool, such that the glass the tool plunges into did not receive direct laser interaction despite the glass being heated for 5 seconds prior to any plunging motion. It is only after moving forward into the workable region that the tool plunges in and displaces in both directions.

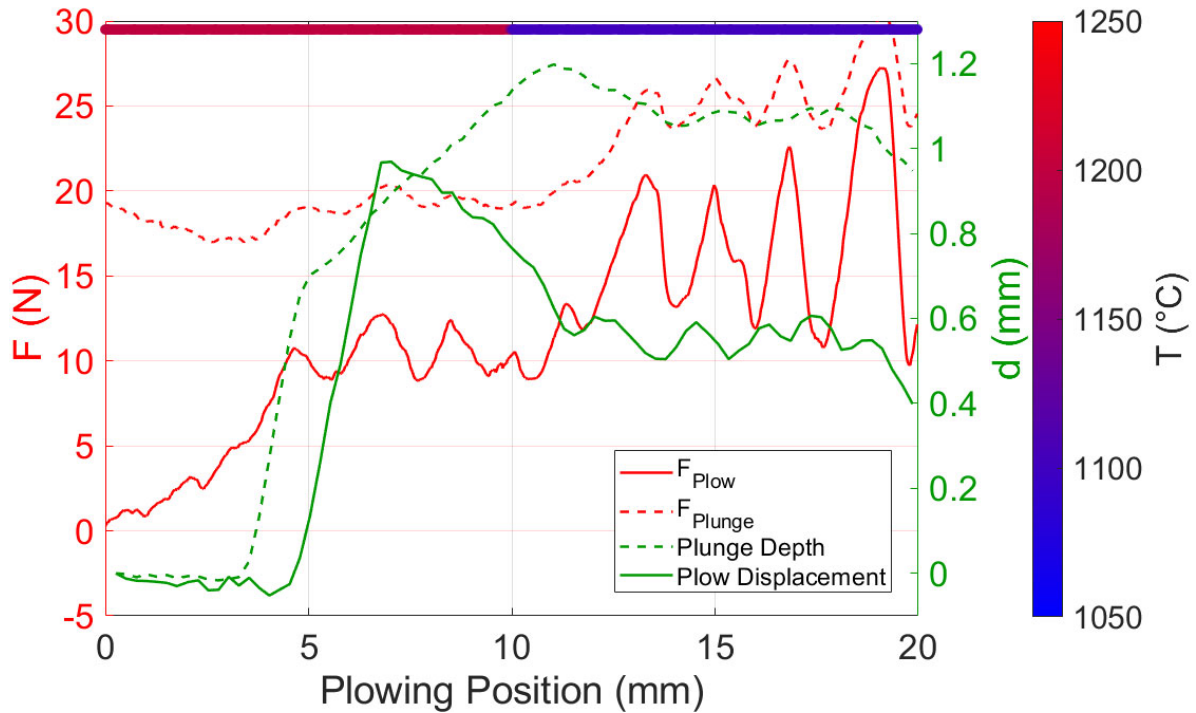


Figure 14: Plot of force (N) and displacement (mm) versus plowing position (mm) for Experiment 2.

The oscillatory nature of the shaping forces and tool displacement is described quantitatively by identifying the spatial frequencies (see Table 1). The average distance between shaping force peaks during the steady state, approximately 5 to 10 mm before the step in reference temperature and 12 to 20 mm after the step, are computed and averaged with the inverse of the result being the spatial frequency. From Table 1 it appears material builds up and is partially released approximately every 2 mm, except for the high temperature region for Experiment 1 where this phenomenon occurs approximately every 1.5 mm.

Table 1: Identified frequency characteristic of temperature step experiments.

Experiment #	Force Type	Dominant Spatial Frequency (cycles/mm)	
		6 - 10 mm Region	12-20 mm Region
1 (1200°C → 1100°C)	Plow Force	0.67	0.54
	Plunge Force	0.73	0.52
2 (1100°C → 1000°C)	Plow Force	0.55	0.53
	Plunge Force	0.53	0.51

Response to Velocity Step

In Experiment 3 the reference temperature is 1200°C and the velocity changes from 0.25 mm/s to 0.5 mm/s after 10 mm of ploughing. Figure 15 shows the shaping forces, measured temperature, plunge depth, and the tool's plow-axis displacement versus displacement along the shaped feature for this experiment. As the scan velocity increases, more glass interacts with the tool per unit time and the shaping forces increase. This is evident in the jump in force once the system approaches a pseudo-steady state value, around 13 mm. Prior to the step, the oscillations do not seem to maintain a steady average value, indicating that the system may not have reached steady state. After the velocity step, a more consistent oscillation pattern develops, indicating steady state is approached. When the velocity is increased, the tool plunges deeper. The tool has a face just less than perpendicular to the substrate surface, such that as the substrate progresses forward, displaced glass material climbs up this face. An increase in velocity increases the amount of material hitting this surface, causing the tool to plunge inward rather than lift the material higher.

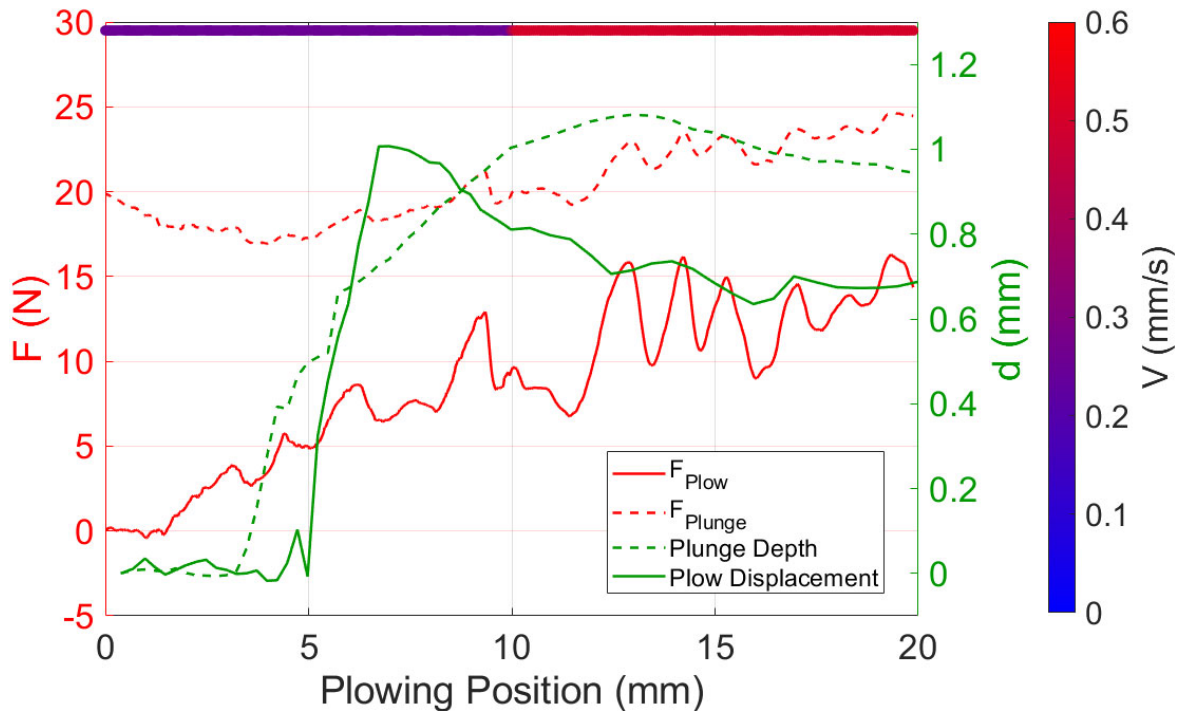


Figure 15: Plot of force (N) and displacement (mm) versus plowing position (mm) for Experiment 3.

In Experiment 4 the reference temperature was 1200°C and the velocity changed from 0.25 mm/s to 0.125 mm/s after 10 mm of ploughing. Figure 16 shows the shaping forces, measured temperature, plunge depth, and the tool's plow-axis displacement versus displacement along the shaped feature for this experiment. In Experiment 4, the tool tip experiences increased shaping forces even though the plough velocity has decreased. This may be due to glass functioning with non-Newtonian behavior, but more experiments must be performed to

investigate this hypothesis. Furthermore, the tooltip is continuously plunging for the first part of the experiment and appeared to reach a steady state when the velocity changed.

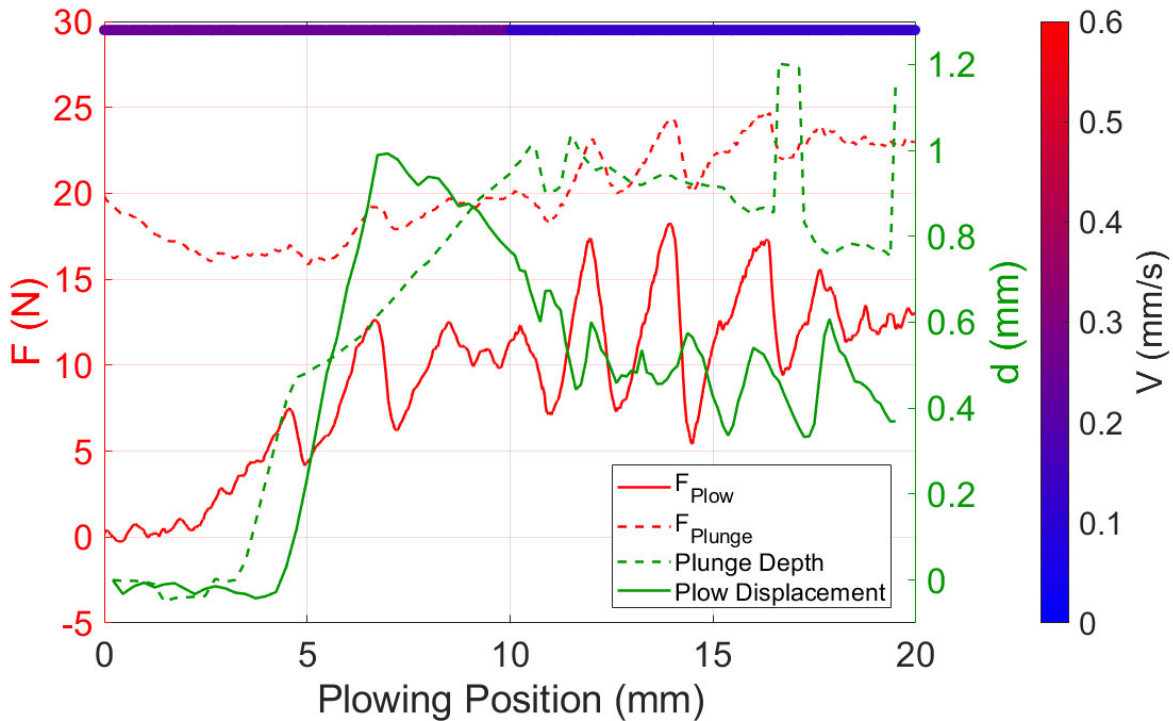


Figure 16: Plot of force (N) and displacement (mm) versus plowing position (mm) for Experiment 4.

A similar investigation into the steady state frequencies found that the values are relatively constant before and after the velocity step for both experiments (see Table 2). The spatial cycle length is 1.39 to 1.89 mm, which is very similar to the values for Experiments 1 and 2 (see Table 1). This suggests that the induced oscillations are not due to the process parameters, but rather the oscillations appear to be due to the movement of the molten material along the tooltip face and how it continuously moves to the sides and then accumulates on the tooltip. This notion is confirmed by the data presented in Table 2. A fast-Fourier transform approach was used to determine the dominant spatial frequency of the track morphology of Experiment 3 from a confocal scan (see Figure 17). The results in the 6-10 mm region, where there was the highest level of signal confidence from the confocal point sensor, closely mirror the spatial frequencies in the force response. This data demonstrates a direct correlation between force and morphology response, validating the approach to sculpt glass with force control techniques.

Table 2: Comparison of spatial frequencies for Experiment 3 in 6-10 mm region.

Force Spatial Frequency	Morphology Spatial Frequency (1/mm)
0.68 cycles/mm	0.675 cycles/mm

Table 3: Identified frequency characteristic of velocity step experiments.

Experiment #	Force Type	Dominant Spatial Frequency (cycles/mm)	
		6 - 10 mm Region	12-20 mm Region
3 (0.25 mm/s → 0.5 mm/s)	Plow	0.68	0.72
	Plunge	0.68	0.72
4 (0.25 mm/s → 0.125 mm/s)	Plow	0.56	0.59
	Plunge	0.53	0.58

The experimental results illustrate that the dynamic shaping forces change exponentially when a process parameter changes in a stepwise manner. To characterize the dynamic shaping process, a first order model is proposed. An average shaping force is determined from the steady regions in the 5 to 10 mm and the 12-20 mm portions of the trench. In Experiments 1 and 2 it is seen that the shaping forces increase as temperature decreases, as seen by the negative gains presented in Table 4. To determine the gain, the change in average force was divided by the step, which related to the temperature (or velocity) changes induced at 10 mm. The time constant was found by identifying the force at which the system was 63% of the final average force beginning at the initial force. In the velocity experiments, the shaping forces increased with both increasing and decreasing velocity. An increase in velocity should logically cause more resistance from the viscous glass, thus, indicating that unmodeled phenomena in Experiment 4 caused the increase in shaping forces.

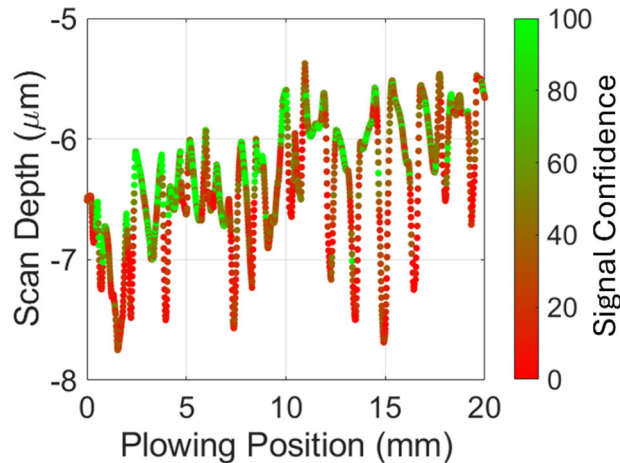


Figure 17: Confocal Scan Morphology of Experiment 3 Track

Table 4: First-order system identification constants.

Experiment	Independent Variable	Force Type	Initial Steady-State Value (N)	Gain (N/°C or N/(mm/s))	Spatial Constant (1/mm)
1	Temperature	Plow	7.4	-0.078	0.9
		Plunge	18.86	-0.064	0.9
2	Temperature	Plow	10.95	-0.065	2.5
		Plunge	19.74	-0.058	2.72
3	Velocity	Plow	8.51	15.36	2.18
		Plunge	18.51	18.08	2.37
4	Velocity	Plow	10.01	-26.96	1.62
		Plunge	18.57	-38.08	1.72

Using the data for Experiment 1, the dynamic response of the plow force is

$$F_1(x) = 15.2e^{-\frac{x}{0.9}} - 7.8 \quad (6)$$

where x is position along the substrate. In Figure 16, this model is implemented to fit the force response. A similar setup exists for experiments 2 and 3 that are obtained by substituting the values from Table 4 into Equation 1. While the data presented in Table 3 would align well with the force responses from Experiment 4, the basic understanding that an increase in velocity increases force demonstrates this specific model is not useful for predicting the force response.

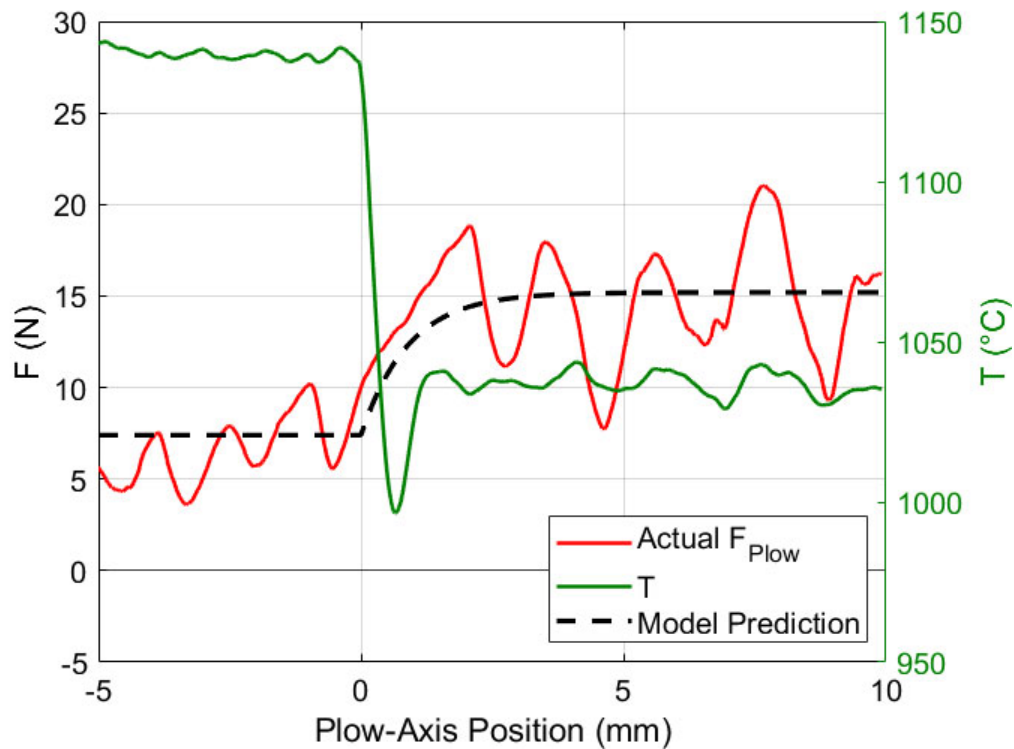


Figure 16: Prediction of plowing response for a -100°C temperature step from Experiment 1.

Figure 18 presents a view of the displacement of glass along the track. The material is not even, but rather ridged. The frequency of these ridges corresponds to the force and tool displacement variations seen in Experiments 1-4. As more experiments are conducted to refine the model, a feedback mechanism will be implemented to maintain constant shaping forces that should produce a more uniform trench morphology.



Figure 18: Morphology of glass substrate at track plowing operations.

Summary and Conclusions

In this paper, initial study of the automated glass shaping process is conducted. In this process a laser heats up a volume of glass in front of a tool that ploughs into the molten glass and displaces it as the part is moved relative to the tool. A real-time control system was constructed that included the temperature sensing and control using a thermal camera, sensing of the forces acting on the tool, and visual sensing of the tool to track its position and the actual plunge depth. These measurements were taken on the same process that controlled the motion system; thus, all data are automatically registered. A series of experiments were conducted to understand the shaping process and how the process variables, namely, velocity and temperature, and the plunge depth affect the shaping forces. The process variables were also changed in a stepwise manner to understand the dynamic response of the shaping force process.

During the temperature step experiments, the key insight observed was that there was an increase in the shaping forces caused by a decrease in temperature. The force induced onto the tool is directly related to the material viscosity, which is determined by temperature for the glass. An increase in temperature makes the glass in the heat zone more workable, which was reflected in both experiments.

The behavior of the velocity step experiments was not consistent. Whether the velocity was decreased or increased, the shaping forces increased. This behavior points at main items to be addressed, longer tests and more research into the viscous behavior of glass. These tests were short in time, spanning no more than 120 seconds. It is possible that at the scale of less than 2 mm of plunge depth, it may take much longer for the system to reach steady state. Further, unmodeled phenomena, particularly the motion of the molten glass, may have affected the results.

The shaping forces had a pronounced oscillatory behavior in the range of 0.5 to 0.75 cycles/mm for all the experiments. The displacement of the tool in the ploughing direction was seen to contain the same spatial frequencies. Upon investigation of the final parts, ridges at the same spatial frequency were present. Therefore, it is believed that glass was exiting the ploughing zone and accumulating on the tool at the same spatial rate. A first order dynamic ploughing force model was fit to the experimental data in Experiment 1. The model describes the steady and dynamic behavior of the ploughing force very well; however, it does not capture the oscillatory behavior of the shaping forces, which may be most strongly influenced by the motion of the work zone.

Going forward, future work must be performed to address the shortcomings of these experiments. Larger scale tests should be conducted to ensure the system is brought to steady state, as the 20 mm of plow travel here appeared insufficient in all of the experiments. A

redesign of the shaping system is required to minimize the tool compliance that allowed for tool displacement on both the plunging and plowing axis as shaping operations were performed. This will allow for better discernment as to whether the oscillatory response of the glass is material or system dependent. Additionally, variation in tool geometry may adjust the glass response.

References

[1] N. Khadka, B. Tiwari, T. Sparks, R.G. Landers, E.C. Kinzel, "Monolithic Glass Forming Using Laser Heated Sculpting," Solid Freeform Fabrication Symposium, Austin, Aug. (2024).

[2] Napolitano, A., & Hawkins, E. G. (1964, May 11). Viscosity of Standard Soda-Lime-Silica Glass. *Journal of Research of National Bureau of Standards*, 68A(5), 1-10.
<https://pmc.ncbi.nlm.nih.gov/articles/PMC6628577/>